Supporting Information

Solvation Structures Dependent Ion Transport and Desolvation Mechanism for Fast-Charging Li-Ion Batteries

Experimental section

Materials

Dimethyl carbonate (DMC, 99.9%, Sigma-Aldrich), diethyl carbonate (DEC, purity ≥ 99.5%, J&K Scientific), 1,3-dioxolane (DOL, purity > 99.8%, Sigma-Aldrich), 2-methyltetrahydrofuran (2-MTHF, 99%, J&K Scientific), 1,2-dimethoxyethane (DME, > 99%, Duoduo reagent), ethylene glycol diethyl ether (DEE, > 98.0%, TCI), ethylene carbonate (EC, >99.0%, TCI), propylene carbonate (PC, purity ≥ 99%, Sigma-Aldrich), and lithium bis(trifluoromethanesulphonyl)imide (LiTFSI, 99.5%, Sigma-Aldrich) were all stored in an Ar-filled glove box (H_2O < 0.1 ppm, O_2 < 1 ppm), where the preparation of electrolytes and the subsequent cell assembly were also performed. The Cu foil, Al foil, lithium anode (d=14mm), $LiFePO_4$ (LFP) electrode powder, $Li_4Ti_5O_{12}$ (LTO) electrode powder, polyvinylidene difluoride (PVDF) binder, and super P were purchased from Guangdong Canrd New Energy Technology Co.,Ltd.. N-methyl-2-pyrrolidone (NMP) was obtained from Aladdin and stored in a cool, dark, and well-ventilated place. All the chemicals were used as received without further purification.

Electrolytes preparation

The electrolytes were prepared by adding 0.2871g LiTFSI into 1ml different solvent (DOL, 2-MTHF, DME, DEE, DMC, DEC, EC, PC) and stirred until the salt was completely dissolved to obtain corresponding electrolytes (DOL Ele., 2-MTHF Ele., DME Ele., DEE Ele., DMC Ele., DEC Ele., EC Ele., PC Ele.).

Electrode preparation

The electrodes were fabricated through the doctor blade coating method with uniform slurry. The LFP cathode slurry was prepared as below. The LFP electrode powder, Super P, and PVDF binder were mixed in NMP with the mass ratio of 8:1:1 to form a slurry first and then coated on the Al foil. The LTO electrode slurry was prepared by uniformly dispersing LTO electrode powder, super P, PVDF binder and TNNDIS with the mass ratio of 8:1:1:0.0005 into NMP. The electrodes were transferred to a vacuum oven and dried at 120 ℃ for 6 hours and then punched into disks with a diameter of 12 mm before use. The areal loading of LFP and LTO electrodes were about 2.8 and 3.3 mg cm^{-2} respectively.

Electrochemical measurements

The LTO||LFP batteries were assembled using Coin 2032-type cells by sandwiching a glass fiber (Whatman GF-A) separator between the LTO anode and LFP cathode with injected 100 μL electrolyte. The charge-discharge cycling test of full cells was performed using LAND CT3002A (Wuhan LAND Electronics Co, Ltd.) at room temperature (RT). All the cells were cycled 5 times between 1.0 ~ 2.5 V at the rates of 1 C, 2 C, 5 C, 8 C, 10 C, 15 C and 20 C, respectively. Electrochemical impedance spectroscopy (EIS) tests were conducted in the frequency range from 10^5 to 10^{-2} Hz with a voltage amplitude of 5 mV, which were carried out with Gamary Interface 1010T at RT.

Stainless steel||stainless steel symmetric cells with a customized polytetrafluoroethylene (PTFE) ring were assembled to measure the ion conductivity (σ) of the electrolytes by

collecting the resistance of bulk electrolyte (R_b) from EIS. the σ is calculated using the equation (1):

$$\sigma = \frac{L}{R_b S} \quad (1)$$

where L is the thickness between two stainless steels (the height of the PTFE ring), S stands for the effective area which is calculated by the inner diameter of the PTFE ring.

The Li^+ transference number (t_{Li}^+) of the electrolyte was obtained via applying the potentiostatic polarization technique on the CHI760e electrochemical workstation using the Bruce-Vincent method. A direct current (DC) pulse of 10 mV was applied to a Li||Li symmetric cell for 300s until the polarization current (R_i) became steady. The EIS measurements were carried out before and after the polarization at 5 mV amplitude voltage range from 10^5 to 10 Hz. The t_{Li}^+ was calculated by the following equation (2):

$$t_{Li^+} = \frac{I_{SS} R_b \left(\Delta V - I_0 R_i^0\right)}{I_0 R_b \left(\Delta V - I_{SS} R_i^{SS}\right)} \quad (2)$$

where ΔV is the applied polarization voltage, I_0 and I_{SS} are the initial current and steady current during the polarization process, while the R_i^0 and R_i^{SS} stand for the interfacial resistance before and after polarization, respectively.

Characterization

^{7}Li Nuclear magnetic resonance (NMR) measurements were performed on a Bruker AVANCE III 400 MHz instrument with 1 M LiCl dissolved in D_2O as an external reference (0 ppm). Fourier transform infrared (FT-IR) spectra were obtained through attenuated total reflection (ATR) mode by directly dripping electrolytes on a diamond single crystal of Bruker instrument range. The wavenumber was from 400-4000 cm^{-1} with accumulating 16 scans per spectra. In/Ex-situ Raman spectra were collected by a confocal Raman microscope (Renishaw inVia-Qontor Raman Microscope) with an excitation wavelength of 532 nm. In ex-situ Raman experiments, electrolytes were stored in 0.5 mm capillaries and the Raman shift ranged from 400-4000 cm^{-1}. In in-situ Raman experiments, a customized in-situ electrochemical cell (**Figure S22a**) was assembled to complete the Raman tests.The Raman signal was collected every 2 seconds from 273 cm^{-1} to 2000 cm^{-1}, with an excitation wavelength of 532 nm, exposuring 1s. As shown in **Figure S22b**, a titanium mesh coated with LTO acts as anodes, and LFP serves as cathodes with a slice of glass fiber filter as separator soaking with abundant electrolytes. The CHI760E electrochemical workstation was used to charge the cell at 10 C with capturing Raman signals.

Theoretical Calculations

Computational methods involved MD simulations of electrolyte structures were realized using the GROMACS 2022 software. Forces were computed employing the Generation Amber Force Field (GAFF). The parameters for Li^+ ions were adopted from the existing force field parameters, while DOL, 2-MTHF, DME, DEE, DMC, DEC, EC, PC, and $TFSI^-$ were generated using ACPYPE[1]. The corresponding atom charges were derived from the restrained electrostatic potential RESP2 charges[2, 3]. The quantities of salt and organic molecules are detailed in Table S3. Atomic partial charges were calculated by fitting the molecular electrostatic potential at atomic centers using Gaussian 16. Topological files and

bonded and Lennard-Jones parameters were generated using Ambertools[4]. Due to the use of a nonpolarizable force field, partial charges for charged ions were scaled in Table S4 to account for electronic screening, which has been shown to improve predictions of interionic interactions[5-7].

The simulation procedure began with an energy minimization using the steepest descent method, followed by a 3 ns equilibration step using a Berendsen barostat[8]. Then, another NVT run of 10 ns was used for analysis, both at a reference pressure of 1 bar with timesteps of 1 fs. A V-rescale thermostat was used throughout with a reference temperature of 298 K. The particle mesh Ewald method was used to calculate electrostatic interactions, and the Verlet cutoff scheme was used to generate pair lists. A cutoff of 1.2 nm was used for nonbonded Lennard-Jones interactions. Periodic boundary conditions were applied in all directions. The convergence of the system energy, temperature, and box size was checked to verify equilibration. The radial distribution functions (RDFs) were calculated using the in-built module, and the snapshot of the MD simulation was produced by VMD software[5].

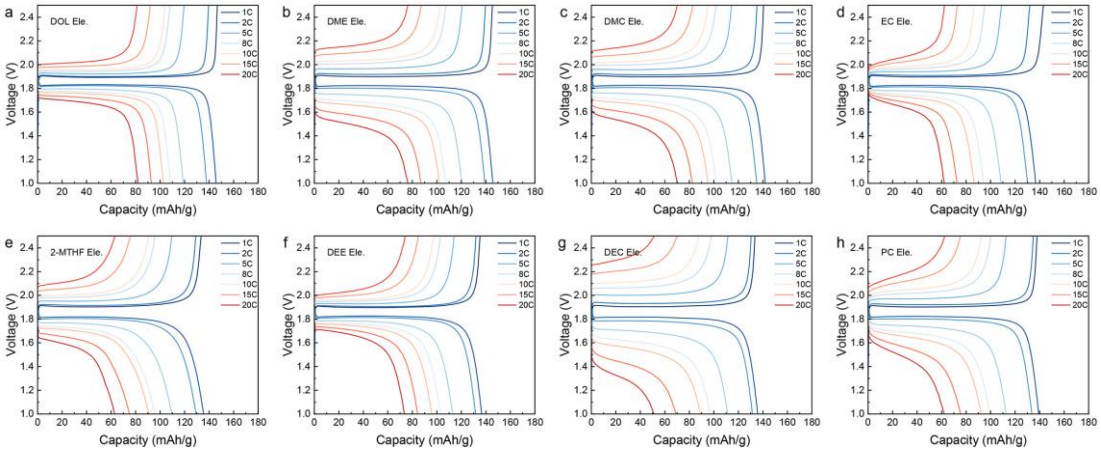

Figure S1. Charge and discharge voltage curves at 1 C, 2 C, 5 C, 8 C, 10 C, 15 C and 20 C with (a) DOL Ele., (b) DME Ele., (c)DMC Ele., (d) EC Ele., (e) 2-MTHF Ele., (f) DEE Ele., (g) DEC Ele., and (h) EC Ele., respectively.

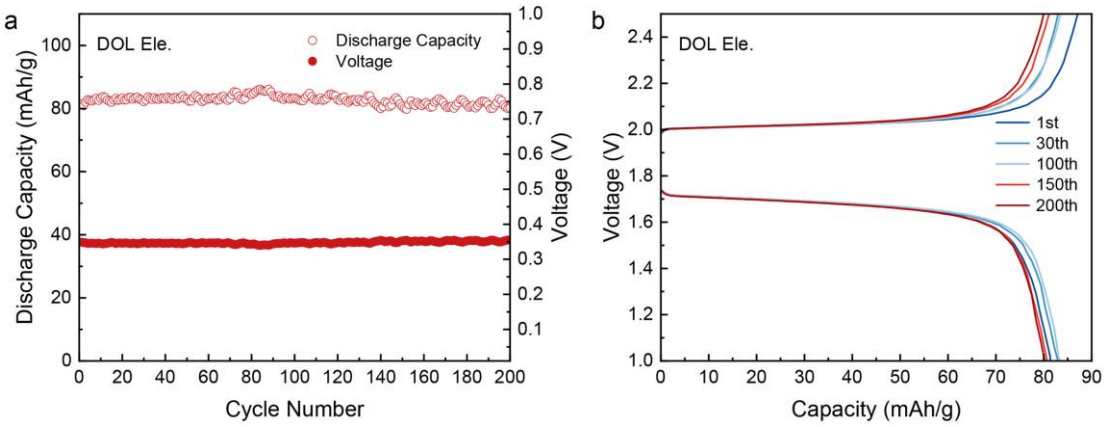

Figure S2. (a) Cycling performance of LTO||LFP full cells with DOL Ele. at 20 C. (b) Charge / discharge curves of 1st, 30th, 100th, 150th and 200th in DOL Ele..

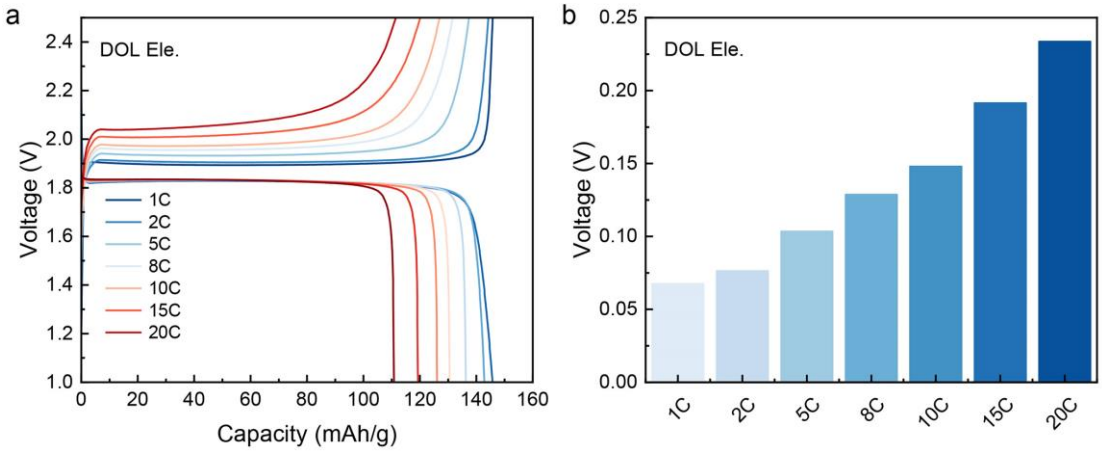

Figure S3. (a) The charge/discharge curves and (b) the corresponding polarization voltage of the LTO||LFP full cell. The cells were charged at 1 C, 2 C, 5 C, 8 C, 10 C 15 C, 20 C and discharged at a constant rate (1 C).

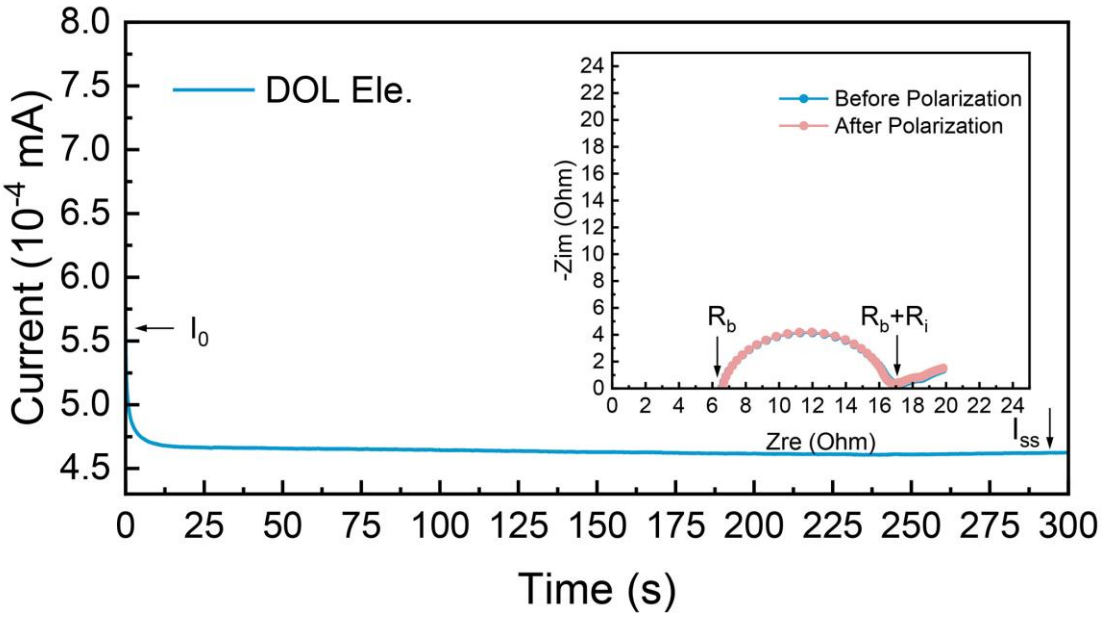

Figure S4. Chronoamperometry curve of Li||Li symmetrical cell with an applied voltage of 10 mV in DOL Ele.. Insets represent the corresponding EIS before and after polarization.

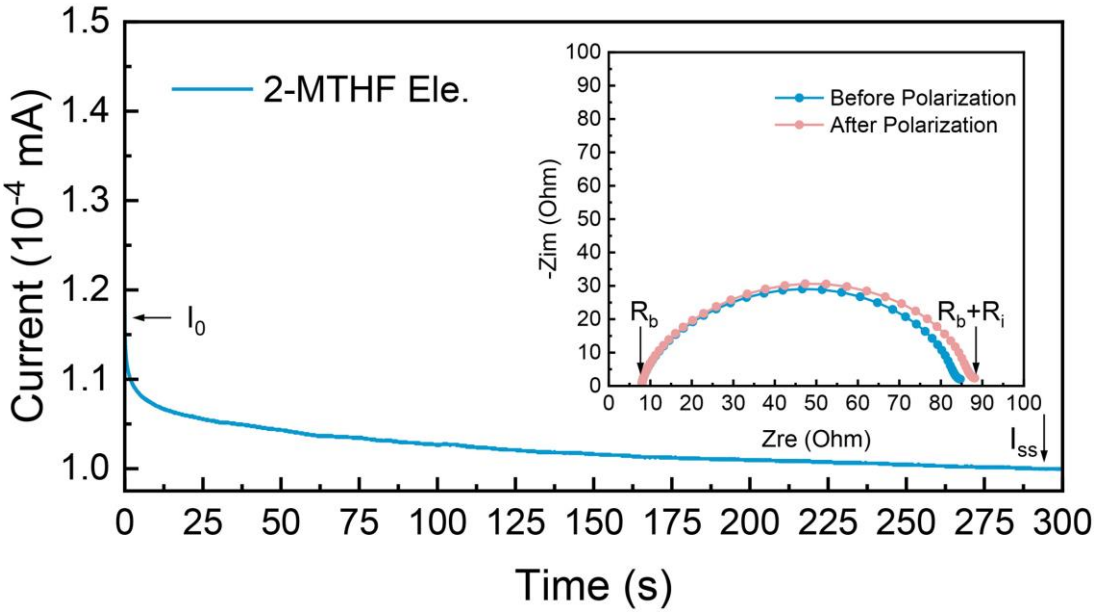

Figure S5. Chronoamperometry curve of Li||Li symmetrical cell with an applied voltage of 10 mV in 2-MTHF Ele.. Insets represent the corresponding EIS before and after polarization.

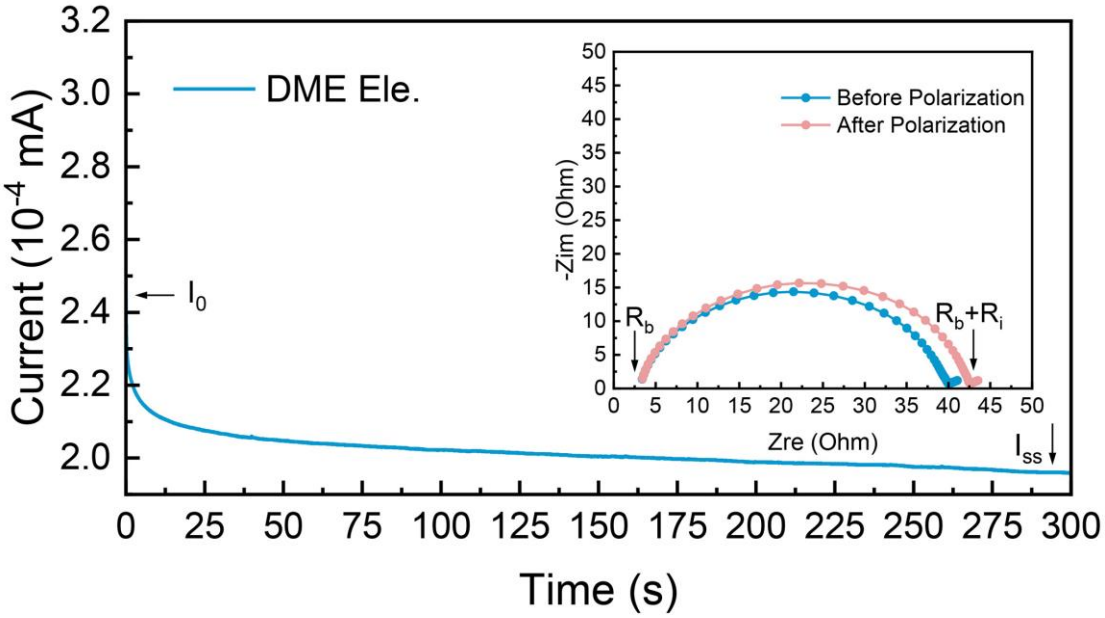

Figure S6. Chronoamperometry curve of Li||Li symmetrical cell with an applied voltage of 10 mV in DME Ele.. Insets represent the corresponding EIS before and after polarization.

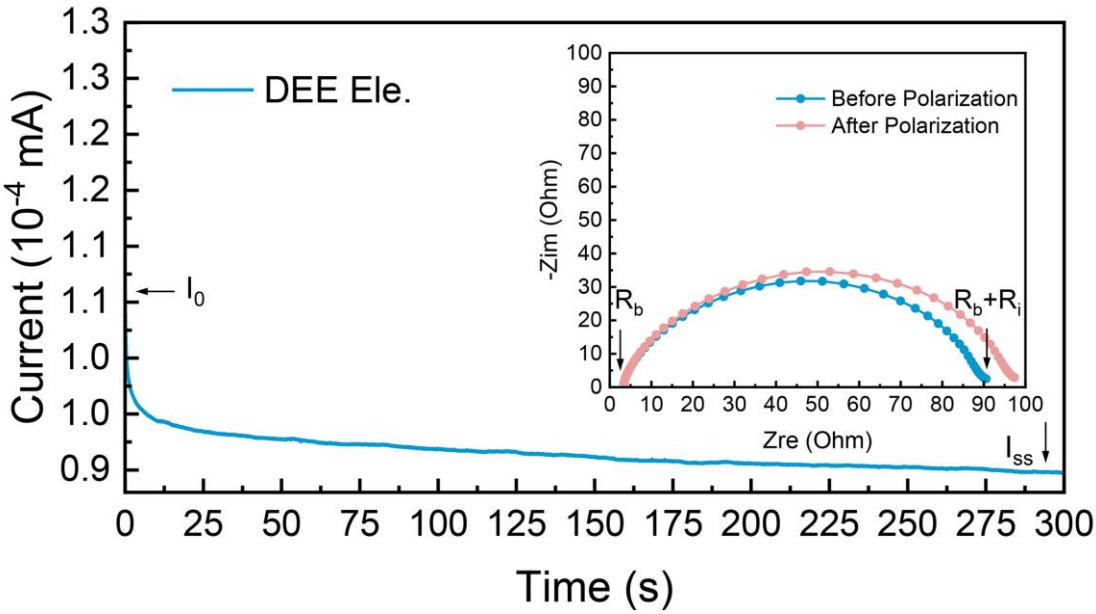

Figure S7. Chronoamperometry curve of Li||Li symmetrical cell with an applied voltage of 10 mV in DEE Ele.. Insets represent the corresponding EIS before and after polarization.

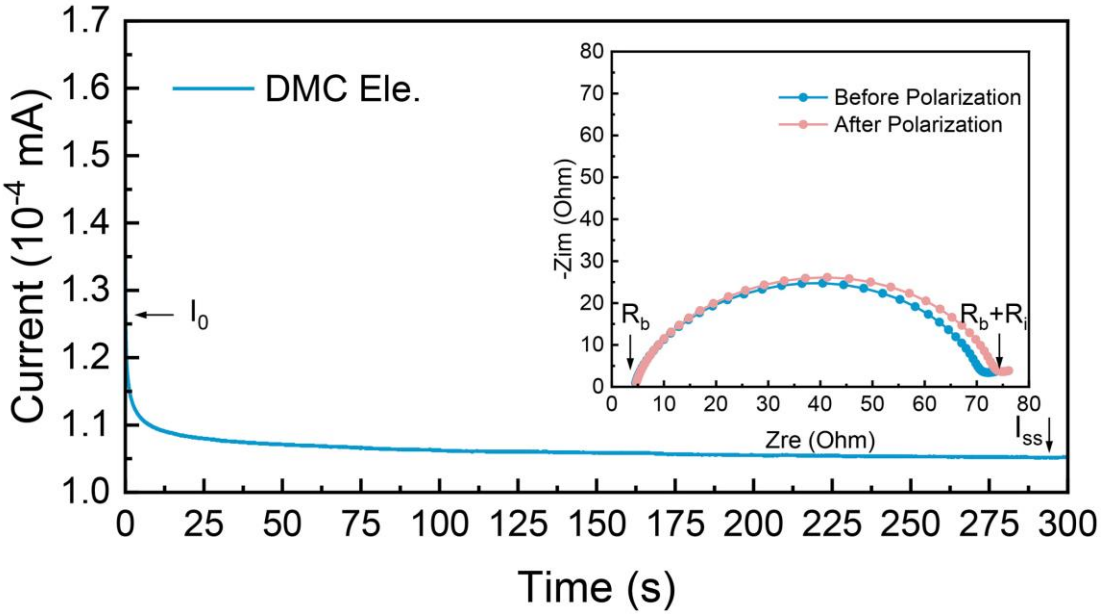

Figure S8. Chronoamperometry curve of Li||Li symmetrical cell with an applied voltage of 10 mV in DMC Ele.. Insets represent the corresponding EIS before and after polarization.

-.

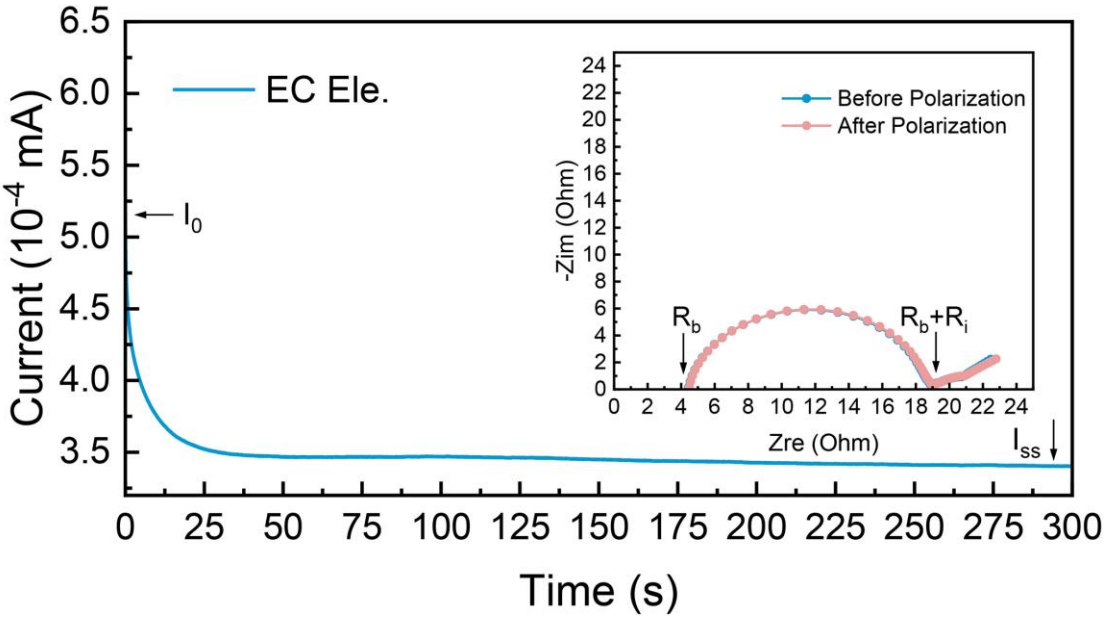

Figure S9. Chronoamperometry curve of Li||Li symmetrical cell with an applied voltage of 10 mV in EC Ele.. Insets represent the corresponding EIS before and after polarization.

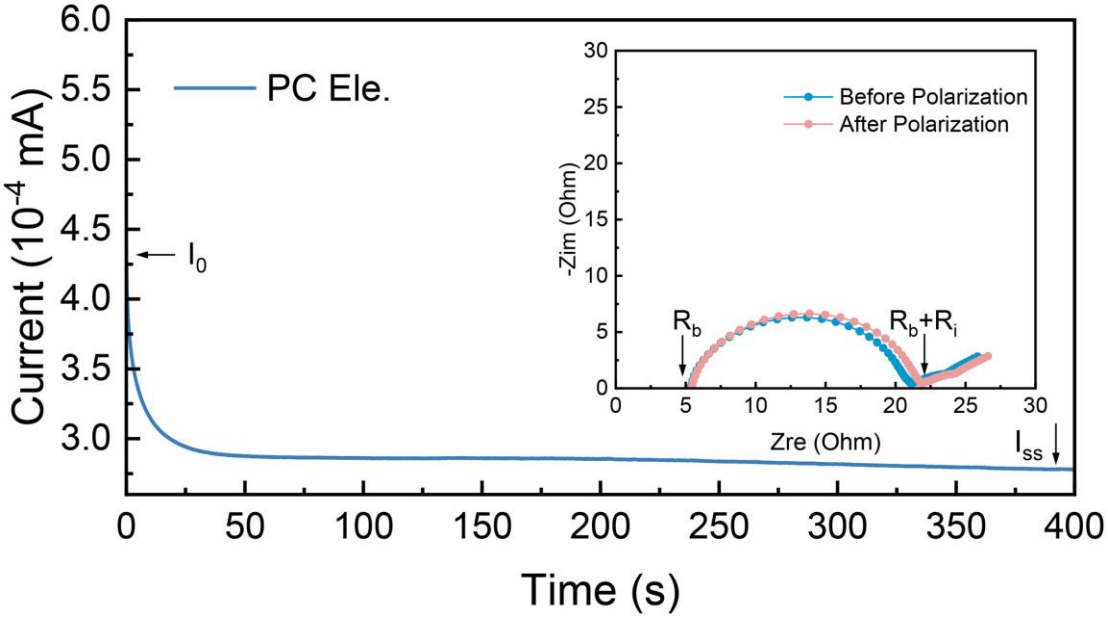

Figure S10. Chronoamperometry curve of Li||Li symmetrical cell with an applied voltage of 10 mV in PC Ele.. Insets represent the corresponding EIS before and after polarization.

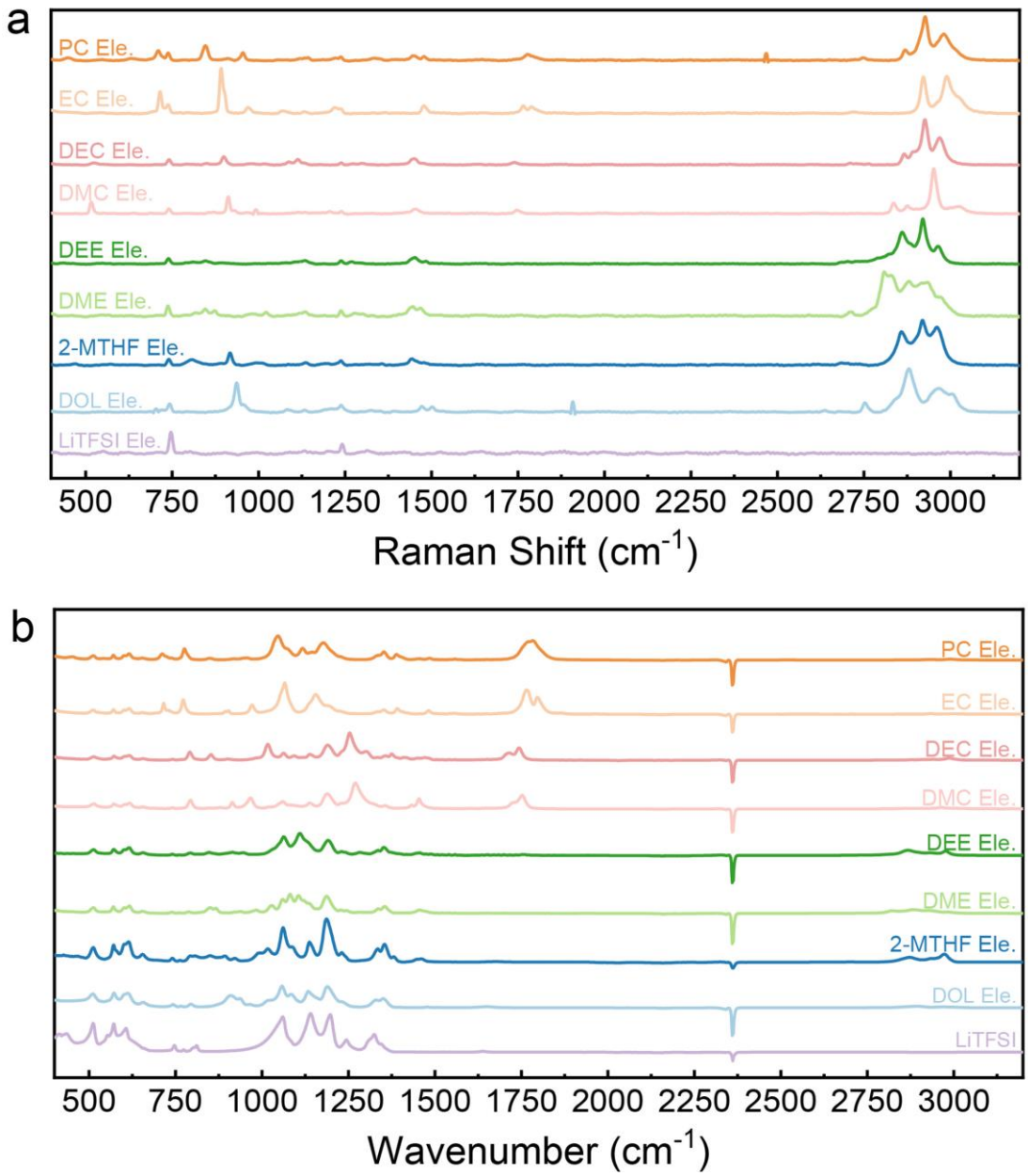

Figure S11. Full range (a) Raman and (b) FT-IR spectra of various electrolytes and LiTFSI salt.

Table S1. Proportions of three solvation structures of different electrolytes obtained by Raman spectroscopy fitting.

Solvent	Ratio of AGG (%)	Ratio of CIP (%)	Ratio of SSIP (%)
DOL Ele.	57.09	47.28	2.62
2-MTHF Ele.	17.50	39.55	42.85
DME Ele.	none	10.13	89.87
DEE Ele.	10.26	55.06	34.68
DMC Ele.	9.56	67.16	23.28
DEC Ele.	18.44	45.31	36.25
EC Ele.	none	6.49	93.51
PC Ele.	none	none	100

Table S2. MD simulation of the coordination number of Li^+ with oxygen in solvents and anions in different electrolytes.

Electrolyte	Solvent	O1	O2	O3	$TFSI^-$	Coordination number
DOL Ele.	DOL	2.895			2.646	5.541
2-MTHF Ele.	2-MTHF	2.914			1.578	4.492
DME Ele.	DME	5.679			0.256	5.935
DEE Ele.	DEE	3.142			1.791	4.933
DMC Ele.	DMC	0.030	3.881		0.752	4.663
DEC Ele.	DEC	0.050	3.677		0.708	4.435
EC Ele.	EC	0.037	4.412		0.042	4.491
PC Ele.	PC	0.016	4.337	0.026	0.049	4.428

*O1, O2 and O3 are labeled in Figure S12.

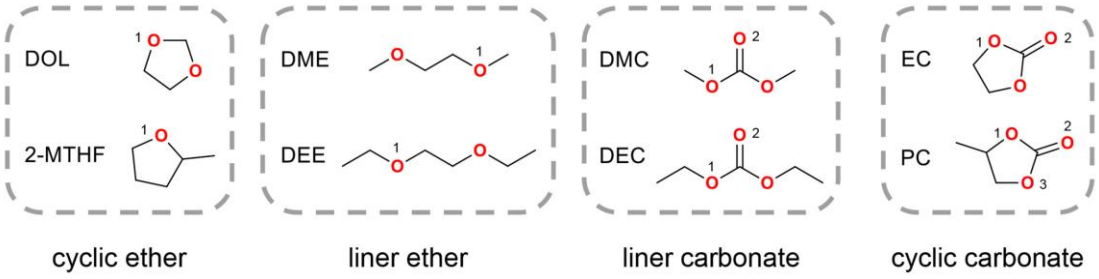

Figure S12. Molecular structures of eight solvents investigated in this work.

Table S3. The number of different solvation structures (AGGs, CIPs, SSIPs), total number and average number of Li^+ in AGG and the number of charges in eight electrolytes extracted from MD simulation.

Electrolyte	SSIP	CIP	AGG	Number of Li^+ in AGG	Average number of Li^+ in AGG	Sum of charge in the solvated structure	Free anions	Sum of charge	Ratio of charge (%)
DOL Ele.	199	2063	3679	13898	3.78	1059	93	1152	0.036
DME Ele.	13154	2708	153	218	1.42	13342	13064	26406	0.821
DMC Ele.	8598	5985	689	1497	2.17	9615	8663	18278	0.568
EC Ele.	15260	803	9	17	1.89	15275	15259	30534	0.949
2-MTHF Ele.	5971	6322	1524	3787	2.48	7789	6489	14278	0.444
DEE Ele.	3536	6475	2497	6069	2.43	5848	3526	9374	0.291
DEC Ele.	7126	7339	859	1615	1.88	8167	6971	15138	0.471
PC Ele.	15972	108	0	0	0	16873	15972	31944	0.993

Table S4. Details of the amount of salt and solvent molecules in 1 M electrolyte extracted from MD simulation.

Electrolyte	Solvent	Number of solvent molecules	Number of Li^+	Number of anions
DOL Ele.	DOL	1145	80	80
DME Ele.	DME	802	80	80
DMC Ele.	DMC	771	80	80
EC Ele.	EC	944	80	80
2-MTHF Ele.	2-MTHF	950	80	80
DEE Ele.	DEE	660	80	80
DEC Ele.	DEC	1200	80	80
PC Ele.	PC	574	80	80

Table S5. Scaling coefficients of charged particles in different electrolytes.

Electrolyte	Scaling Coefficients
DOL Ele.	0.714184
DME Ele.	0.711238
DMC Ele.	0.724853
EC Ele.	0.704473
2-MTHF Ele.	0.73062
DEE Ele.	0.723118
DEC Ele.	0.704473
PC Ele.	0.721501

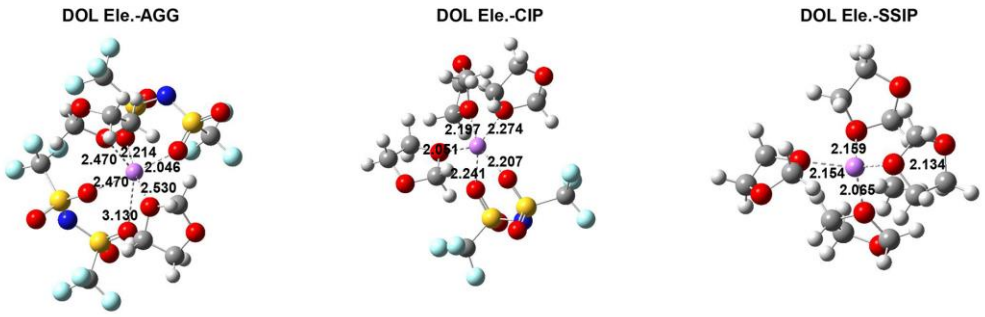

Figure S13. Representative configuration of solvation structures in DOL Ele.. Li, O, C, S, N, F and H atoms are shown are purple, red, gray, yellow, blue, cyan and lightgray, respectively.

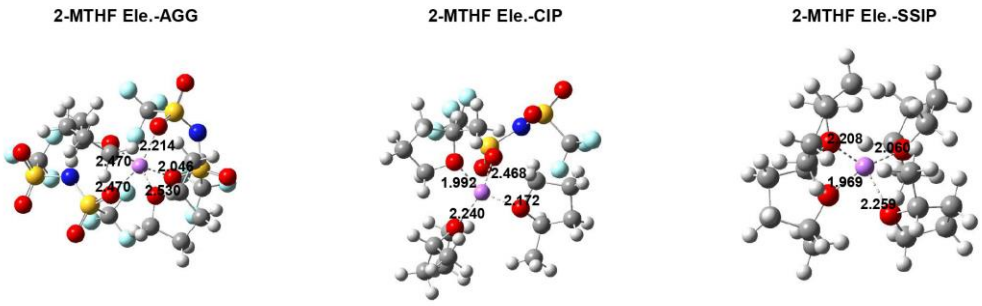

Figure S14. Representative configuration of solvation structures in 2-MTHF Ele.. Li, O, C, S, N, F and H atoms are shown are purple, red, gray, yellow, blue, cyan and lightgray, respectively.

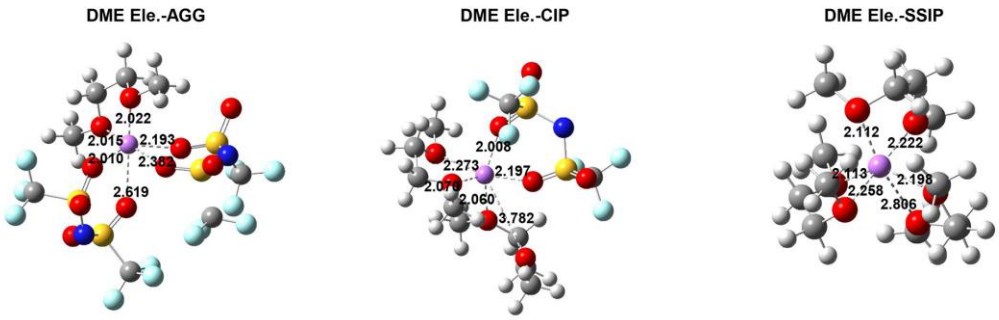

Figure S15. Representative configuration of solvation structures in DME Ele.. Li, O, C, S, N, F and H atoms are shown are purple, red, gray, yellow, blue, cyan and lightgray, respectively.

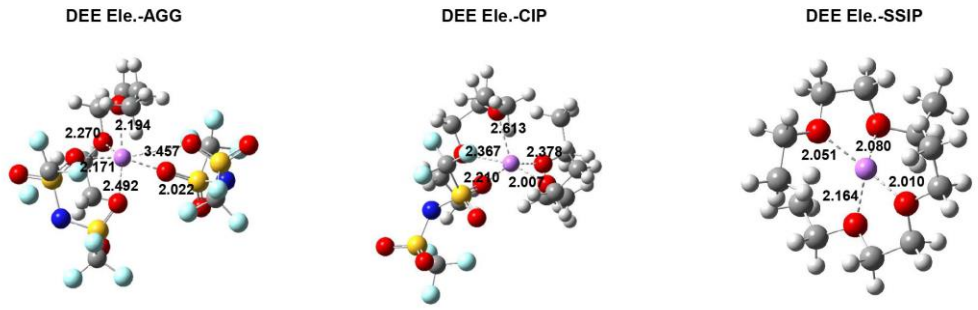

Figure S16. Representative configuration of solvation structures in DEE Ele.. Li, O, C, S, N, F and H atoms are shown are purple, red, gray, yellow, blue, cyan and lightgray, respectively.

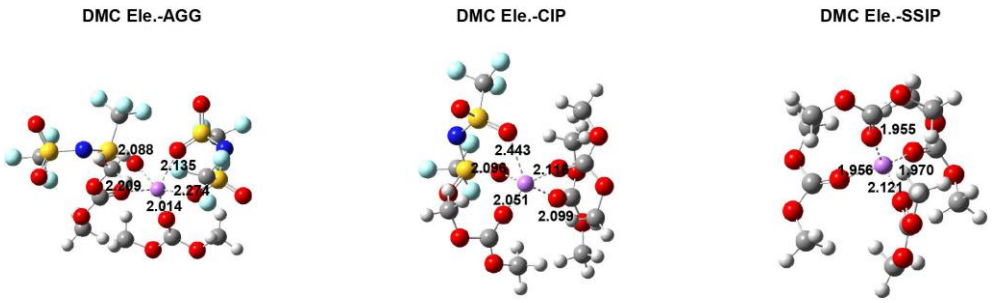

Figure S17. Representative configuration of solvation structures in DMC Ele.. Li, O, C, S, N, F and H atoms are shown are purple, red, gray, yellow, blue, cyan and lightgray, respectively.

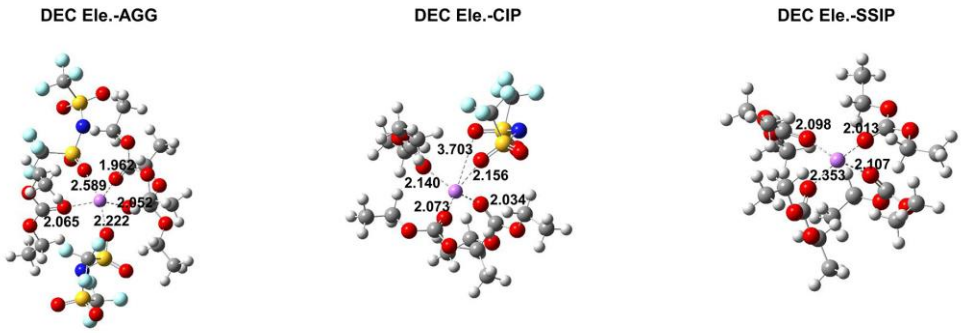

Figure S18. Representative configuration of solvation structures in DEC Ele.. Li, O, C, S, N, F and H atoms are shown are purple, red, gray, yellow, blue, cyan and lightgray, respectively.

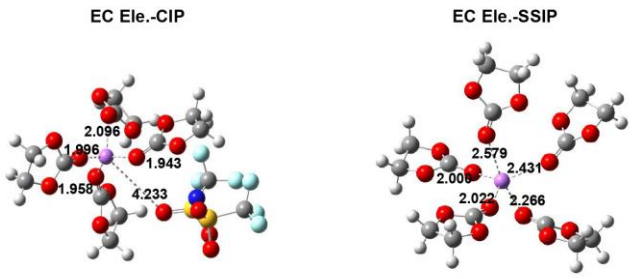

Figure S19. Representative configuration of solvation structures in EC Ele.. Li, O, C, S, N, F and H atoms are shown are purple, red, gray, yellow, blue, cyan and lightgray, respectively.

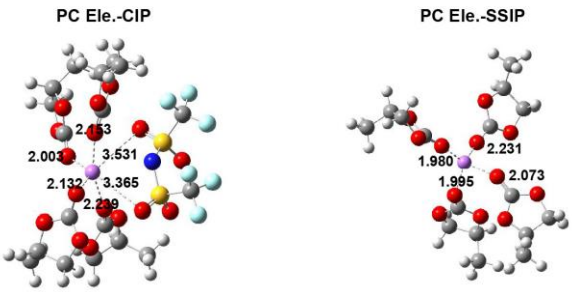

Figure S20. Representative configuration of solvation structures in PC Ele.. Li, O, C, S, N, F and H atoms are shown are purple, red, gray, yellow, blue, cyan and lightgray, respectively.

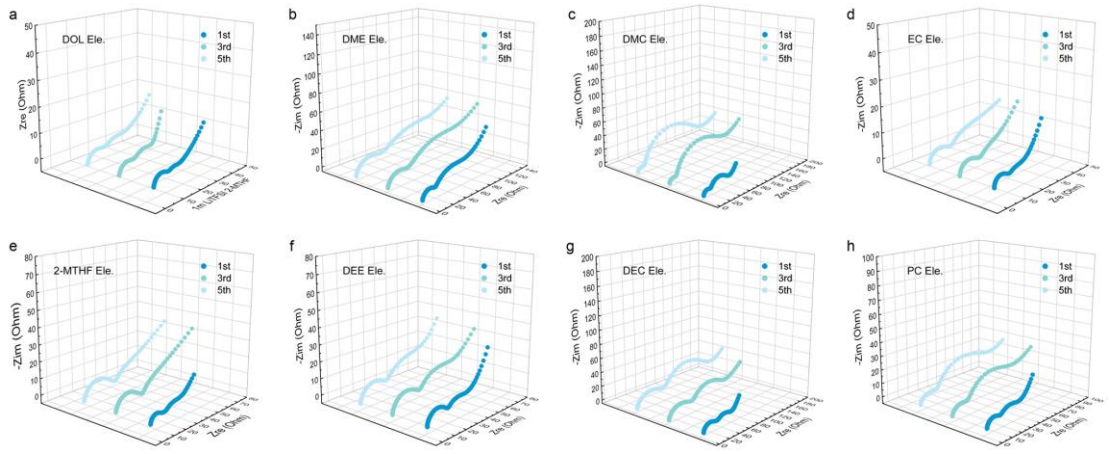

Figure S21. EIS analysis of LTO||LFP batteries in (a) DOL Ele., (b) DME Ele., (c) DMC Ele., (d) EC Ele., (e) 2-MTHF Ele., (f) DEE Ele., (g) DEC Ele. and (h) PC Ele.. The batteries were charged and discharged at 1C, and the EIS data of the charging platform was collected during the 1st, 3rd and 5th cycles.

Table S6. The electrochemical impedance parameters R_b, R_{SEI} and R_{CT} in different electrolytes fitted based on the equivalent circuit model.

electrolyte	1st			3rd			5th		
	$R_b(\Omega)$	$R_{SEI}(\Omega)$	$R_{CT}(\Omega)$	$R_b(\Omega)$	$R_{SEI}(\Omega)$	$R_{CT}(\Omega)$	$R_b(\Omega)$	$R_{SEI}(\Omega)$	$R_{CT}(\Omega)$
DOL Ele.	3.894	5.624	7.773	4.02	6.122	12.44	3.997	6.925	12.96
DME Ele.	1.978	14.73	50.22	1.972	23.28	76.37	1.942	30.03	72.22
DMC Ele.	3.527	11.17	36.67	3.627	10.59	83.73	3.335	10.12	100.8
EC Ele.	3.082	6.01	11.01	2.934	7.569	36.26	3.901	8.546	25.4
2-MTHF Ele.	5.789	8.498	22.46	5.792	18.66	40.66	5.786	22.29	34.67
DEE Ele.	2.797	15.03	19.51	2.7	19.44	23.7	2.769	18.82	36.91
DEC Ele.	5.507	21.16	37.4	5.523	40.35	75.08	5.608	46.78	99.49
PC Ele.	3.402	11.19	22.45	3.416	12.77	44.94	3.452	13.23	53.67

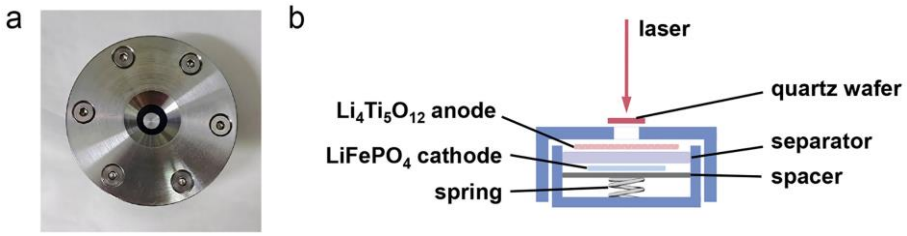

Figure S22. (a) Digital image and (b) schematic diagram of in-situ Raman electrochemical cell.

REFERENCES

1. A. W. Sousa da Silva and W. F. Vranken, ACPYPE - AnteChamber PYthon Parser interfacE, *BMC Res. Notes*, 2012, **5**, 367.
2. C. I. Bayly, P. Cieplak, W. Cornell and P. A. Kollman, A well-behaved electrostatic potential based method using charge restraints for deriving atomic charges: the RESP model, *The Journal of Physical Chemistry*, 2002, **97**, 10269-10280.
3. M. Schauperl, P. S. Nerenberg, H. Jang, L. P. Wang, C. I. Bayly, D. L. Mobley and M. K. Gilson, Non-bonded force field model with advanced restrained electrostatic potential charges (RESP2), *Commun. Chem.*, 2020, **3**, 44.
4. Y. Duan, C. Wu, S. Chowdhury, M. C. Lee, G. Xiong, W. Zhang, R. Yang, P. Cieplak, R. Luo, T. Lee, J. Caldwell, J. Wang and P. Kollman, A point-charge force field for molecular mechanics simulations of proteins based on condensed-phase quantum mechanical calculations, *J. Comput. Chem.*, 2003, **24**, 1999-2012.
5. W. Humphrey, A. Dalke and K. Schulten, VMD: Visual molecular dynamics, *J. Mol. Graph.*, 1996, **14**, 33-38.
6. I. Leontyev and A. Stuchebrukhov, Accounting for electronic polarization in non-polarizable force fields, *Phys. Chem. Chem. Phys.*, 2011, **13**, 2613-2626.
7. I. V. Leontyev and A. A. Stuchebrukhov, Polarizable molecular interactions in condensed phase and their equivalent nonpolarizable models, *J. Chem. Phys.*, 2014, **141**, 014103.
8. H. J. C. Berendsen, D. van der Spoel and R. van Drunen, GROMACS: A message-passing parallel molecular dynamics implementation, *Comput. Phys. Commun.*, 1995, **91**, 43-56.